The Astrophysical Journal Letters, 889:L34 (8pp), 2020 February 1 https://doi.org/10.3847/2041-8213/ab6443

Detection and Characterization of Oscillating Red Giants: First Results from the *TESS* Satellite

Víctor Silva Aguirre[1], Dennis Stello[1,2,3], Amalie Stokholm[1], Jakob R. Mosumgaard[1], Warrick H. Ball[1,4], Sarbani Basu[5], Diego Bossini[6], Lisa Bugnet[7,8], Derek Buzasi[9], Tiago L. Campante[6,10], Lindsey Carboneau[9], William J. Chaplin[1,4], Enrico Corsaro[11], Guy R. Davies[1,4], Yvonne Elsworth[1,4], Rafael A. García[7,8], Patrick Gaulme[12,13], Oliver J. Hall[1,4], Rasmus Handberg[1], Marc Hon[2], Thomas Kallinger[14], Liu Kang[15], Mikkel N. Lund[1], Savita Mathur[16,17], Alexey Mints[18], Benoit Mosser[19], Zeynep Çelik Orhan[20], Thaíse S. Rodrigues[21], Mathieu Vrard[6,22], Mutlu Yıldız[20], Joel C. Zinn[2,22,23], Sibel Örtel[20], Paul G. Beck[16,17,24], Keaton J. Bell[25,62], Zhao Guo[26], Chen Jiang[27], James S. Kuszlewicz[12], Charles A. Kuehn[28], Tanda Li[1,3,4], Mia S. Lundkvist[1], Marc Pinsonneault[22], Jamie Tayar[29,63], Margarida S. Cunha[4,6], Saskia Hekker[1,12], Daniel Huber[29], Andrea Miglio[1,4], Mario J. P. F. G. Monteiro[6,10], Ditte Slumstrup[1,30], Mark L. Winther[1], George Angelou[31], Othman Benomar[32,33], Attila Bódi[34,35], Bruno L. De Moura[36], Sébastien Deheuvels[37], Aliz Derekas[34,38,39], Maria Pia Di Mauro[40], Marc-Antoine Dupret[41], Antonio Jiménez[16,17], Yveline Lebreton[19,42], Jaymie Matthews[43], Nicolas Nardetto[44], Jose D. do Nascimento, Jr.[45,46], Filipe Pereira[6,10], Luisa F. Rodríguez Díaz[1], Aldo M. Serenelli[47,48], Emanuele Spitoni[1], Edita Stonkutė[49], Juan Carlos Suárez[50,51], Robert Szabó[34,35], Vincent Van Eylen[52], Rita Ventura[11], Kuldeep Verma[1], Achim Weiss[31], Tao Wu[53,54,55], Thomas Barclay[56,57], Jørgen Christensen-Dalsgaard[1], Jon M. Jenkins[58], Hans Kjeldsen[1], George R. Ricker[59], Sara Seager[59,60,61], and Roland Vanderspek[59]

[1] Stellar Astrophysics Centre (SAC), Department of Physics and Astronomy, Aarhus University, Ny Munkegade 120, DK-8000 Aarhus C, Denmark
victor@phys.au.dk
[2] School of Physics, The University of New South Wales, Sydney, NSW 2052, Australia
[3] Sydney Institute for Astronomy (SIfA), School of Physics, University of Sydney, Sydney, NSW 2006, Australia
[4] School of Physics and Astronomy, University of Birmingham, Birmingham B15 2TT, UK
[5] Department of Astronomy, Yale University, New Haven, CT 06520, USA
[6] Instituto de Astrofísica e Ciências do Espaço, Universidade do Porto, Rua das Estrelas, 4150-762 Porto, Portugal
[7] IRFU, CEA, Université Paris-Saclay, F-91191 Gif-sur-Yvette, France
[8] AIM, CEA, CNRS, Université Paris-Saclay, Université Paris Diderot, Sorbonne Paris Cité, F-91191 Gif-sur-Yvette, France
[9] Dept. of Chemistry and Physics, Florida Gulf Coast University, 10501 FGCU Boulevard South, Fort Myers, FL 33965, USA
[10] Departamento de Física e Astronomia, Faculdade de Ciências da Universidade do Porto, Rua do Campo Alegre, s/n, 4169-007 Porto, Portugal
[11] INAF—Osservatorio Astrofisico di Catania, Via S. Sofia, 78, I-95123 Catania, Italy
[12] Max Planck Institute for Solar System Research, Justus-von-Liebig Weg 3, D-37077 Göttingen, Germany
[13] Department of Astronomy, New Mexico State University, P.O. Box 30001, MSC 4500, Las Cruces, NM 88003-8001, USA
[14] Institut für Astrophysik, Universität Wien, Türkenschanzstrasse 17, A-1180 Vienna, Austria
[15] Department of Astronomy, Beijing Normal University, 100875 Beijing, People's Republic of China
[16] Instituto de Astrofísica de Canarias, E-38200 La Laguna, Tenerife, Spain
[17] Departamento de Astrofísica, Universidad de La Laguna, E-38206 La Laguna, Tenerife, Spain
[18] Leibniz-Institut für Astrophysik Potsdam (AIP), An der Sternwarte 16, D-14482 Potsdam, Germany
[19] LESIA, Observatoire de Paris, Université PSL, CNRS, Sorbonne Université, Université de Paris, F-92195 Meudon, France
[20] Department of Astronomy and Space Sciences, Science Faculty, Ege University, 35100, Bornova, İzmir, Turkey
[21] Osservatorio Astronomico di Padova—INAF, Vicolo dell'Osservatorio 5, I-35122 Padova, Italy
[22] Department of Astronomy, The Ohio State University, 140 West 18th Avenue, Columbus, OH 43210, USA
[23] Kavli Institute for Theoretical Physics, University of California, Santa Barbara, CA 93106, USA
[24] Institute of Physics, Karl-Franzens University of Graz, NAWI Graz, Universitätsplatz 5/II, A-8010 Graz, Austria
[25] DIRAC Institute, Department of Astronomy, University of Washington, Seattle, WA 98195-1580, USA
[26] Center for Exoplanets and Habitable Worlds, Department of Astronomy and Astrophysics, 525 Davey Laboratory, The Pennsylvania State University, University Park, PA16802, USA
[27] School of Physics and Astronomy, Sun Yat-Sen University, No. 135, Xingang Xi Road, Guangzhou, 510275, People's Republic of China
[28] Department of Physics and Astronomy, University of Northern Colorado, Greeley, CO 80639, USA
[29] Institute for Astronomy, University of Hawaii, 2680 Woodlawn Drive, Honolulu, HI 96822, USA
[30] European Southern Observatory, Alonso de Córdova 3107, Vitacura, Santiago, Chile
[31] Max-Planck-Institut für Astrophysics, Karl Schwarzschild Strasse 1, D-85748, Garching, Germany
[32] Solar Science Observatory, NAOJ, Mitaka, Japan
[33] Center for Space Science, New York University Abu Dhabi, Abu Dhabi, UAE
[34] Konkoly Observatory, Research Centre for Astronomy and Earth Sciences, H-1121 Budapest, Konkoly Thege M. út 15-17, Hungary
[35] MTA CSFK Lendület Near-Field Cosmology Research Group, Hungary
[36] Instituto Federal do R.G. do Norte - IFRN, Brazil
[37] IRAP, Université de Toulouse, CNRS, CNES, UPS, Toulouse, France
[38] ELTE Eötvös Loránd University, Gothard Astrophysical Observatory, Szombathely, Hungary
[39] MTA-ELTE Exoplanet Research Group, 9700 Szombathely, Szent Imre h.u. 112, Hungary
[40] INAF-IAPS, Istituto di Astrofisica e Planetologia Spaziali, Via del Fosso del Cavaliere 100, I-00133 Roma, Italy
[41] STAR Institute, University of Liège, 19C Allée du 6 Août, B-4000 Liège, Belgium
[42] Univ Rennes, CNRS, IPR (Institut de Physique de Rennes) - UMR 6251, F-35000 Rennes, France
[43] Department of Physics and Astronomy, University of British Columbia, Vancouver, Canada
[44] Université Côte d'Azur, Observatoire de la Côte d'Azur, CNRS, Laboratoire Lagrange, France
[45] Universidade Federal do Rio Grande do Norte, UFRN, Departamento de Física, 59078-970, Natal, RN, Brazil
[46] Harvard-Smithsonian Center for Astrophysics, 60 Garden Street, Cambridge, MA 02138, USA
[47] Instituto de Ciencias del Espacio (ICE, CSIC), Campus UAB, Carrer de Can Magrans, s/n, E-08193 Cerdanyola del Valles, Spain
[48] Institut d'Estudis Espacials de Catalunya (IEEC), Gran Capita 4, E-08034, Barcelona, Spain

[49] Institute of Theoretical Physics and Astronomy, Vilnius University, Saulėtekio al. 3, 10257 Vilnius, Lithuania
[50] Dept. Física Teórca y del Cosmos, Universidad de Granada, E-18006 Granada, Spain
[51] Instituto de Astrofísicaísica de Andalucía (CSIC), Glorieta de la Astronomía s/n, E-18008 Granada, Spain
[52] Mullard Space Science Laboratory, University College London, Holmbury St Mary, Dorking RH5 6NT, UK
[53] Yunnan Observatories, Chinese Academy of Sciences, 396 Yangfangwang, Guandu District, Kunming, 650216, People's Republic of China
[54] Key Laboratory for the Structure and Evolution of Celestial Objects, Chinese Academy of Sciences, 396 Yangfangwang, Guandu District, Kunming, 650216, People's Republic of China
[55] Center for Astronomical Mega-Science, Chinese Academy of Sciences, 20A Datun Road, Chaoyang District, Beijing, 100012, People's Republic of China
[56] NASA Goddard Space Flight Center, 8800 Greenbelt Road, Greenbelt, MD 20771, USA
[57] University of Maryland, Baltimore County, 1000 Hilltop Circle, Baltimore, MD 21250, USA
[58] NASA Ames Research Center, Moffett Field, CA 94035, USA
[59] Department of Physics and Kavli Institute for Astrophysics and Space Research, Massachusetts Institute of Technology, Cambridge, MA 02139, USA
[60] Department of Earth, Atmospheric and Planetary Sciences, Massachusetts Institute of Technology, Cambridge, MA 02139, USA
[61] Department of Aeronautics and Astronautics, Massachusetts Institute of Technology, 77 Massachusetts Avenue, Cambridge, MA 02139, USA
Received 2019 November 13; revised 2019 December 9; accepted 2019 December 14; published 2020 January 29

Abstract

Since the onset of the "space revolution" of high-precision high-cadence photometry, asteroseismology has been demonstrated as a powerful tool for informing Galactic archeology investigations. The launch of the NASA *Transiting Exoplanet Survey Satellite* (*TESS*) mission has enabled seismic-based inferences to go full sky—providing a clear advantage for large ensemble studies of the different Milky Way components. Here we demonstrate its potential for investigating the Galaxy by carrying out the first asteroseismic ensemble study of red giant stars observed by *TESS*. We use a sample of 25 stars for which we measure their global asteroseimic observables and estimate their fundamental stellar properties, such as radius, mass, and age. Significant improvements are seen in the uncertainties of our estimates when combining seismic observables from *TESS* with astrometric measurements from the *Gaia* mission compared to when the seismology and astrometry are applied separately. Specifically, when combined we show that stellar radii can be determined to a precision of a few percent, masses to 5%–10%, and ages to the 20% level. This is comparable to the precision typically obtained using end-of-mission *Kepler* data.

Unified Astronomy Thesaurus concepts: Asteroseismology (73); Fundamental parameters of stars (555); Red giant stars (1372)

Supporting material: machine-readable table

1. Introduction

Asteroseismology of red giant stars has been one of the major successes of the *CoRoT* and *Kepler* missions. The unambiguous detection of non-radial oscillations has fundamentally widened our understanding of the inner workings of red giants, including the conditions in their core (e.g., Bedding et al. 2011). The observed frequency spectra have allowed the determination of the physical properties of thousands of red giants to an unprecedented level of precision (e.g., Miglio et al. 2013), paving the way for the emergence of asteroseismology as a powerful tool for Milky Way studies and Galactic archeology (e.g., Miglio et al. 2009; Casagrande et al. 2016; Anders et al. 2017; Silva Aguirre et al. 2018; Sharma et al. 2019). The *Transiting Exoplanet Survey Satellite* (*TESS*; Ricker et al. 2015) is on the path of continuing this legacy with its all-sky survey that is expected to increase the number of detected oscillating red giants by an order of magnitude compared to the tens of thousands reported by its predecessors *CoRoT* and *Kepler*.

In the nominal *TESS* mission, the ecliptic northern and southern hemispheres are each observed during thirteen 27 day-long sectors, and most (92%) of the surveyed sky will be monitored for just 1–2 sectors. Except for the 20,000 targets pre-selected in each sector for 2 minutes cadence observations, all stars are observed as part of the full-frame images obtained in 30 minutes cadence, similar to the long-cadence sampling of the *Kepler* satellite. The length of the observations sets the lower limit on the oscillation frequencies one can resolve, and the sampling sets the upper frequency limit. We know from previous *Kepler* observations that one month of 30 minutes cadence data should be well suited to detect oscillations in the low red-giant branch and sufficient to measure the global oscillation properties characterizing the frequency spectrum, in particular, its frequency of maximum power, $\nu_{\rm max}$, and the frequency separation between overtone modes, $\Delta\nu$ (Bedding et al. 2010). These in turn can be used in combination with complementary data such as the effective temperature, $T_{\rm eff}$, the relative iron abundance, [Fe/H], and parallax, to obtain precise stellar properties (including ages) when applying asteroseismic-based grid modeling approaches (see, e.g., Rodrigues et al. 2017; Pinsonneault et al. 2018).

Due to the large sky coverage, approximately 97% of asteroseismic detections in red giants from the *TESS* nominal mission data are expected to come from stars observed for only one or two sectors.[64] Here we set out to explore the capability of *TESS* to detect the oscillations in giants ranging from the base of the red giant branch to the red clump, determine their stellar properties, and use that to assess the prospects for Galactic archeology studies using one to two sectors of *TESS* data.

2. Target Selection

Our goal is to have a representative sample of giants including the types of stars in which we can expect to detect

[62] NSF Astronomy and Astrophysics Postdoctoral Fellow and DIRAC Fellow.
[63] Hubble Fellow.

[64] Based on a preliminary simulation of the full *TESS* sky (TESS GI Proposal No. G011188).

oscillations from one sector 30 minutes cadence *TESS* data. We selected red-giant candidates observed during sectors 1 and/or 2 that were deemed viable for asteroseismic detections according to their predicted properties based on the *Hipparcos* catalog (Van Leeuwen 2007). We first estimated the stellar $T_{\rm eff}$ and luminosity using B–V color, V-band, and *Hipparcos* parallax, and the color-temperature and bolometric correction relations of Flower (1996). We then obtained a prediction of $\nu_{\rm max}$ ($\propto T_{\rm eff}^{3.5}\ M/L$; solar scaled, e.g., Yu et al. 2018) for each star assuming a mass of 1.2 $M_{\odot}$, which is representative of a typical red giant as observed by *Kepler* (and unlikely to be more than a factor of two from the true value of each star, e.g., Yu et al. 2018). We note that one of our targets (TIC 129649472) is a known exoplanet host star recently analyzed by Campante et al. (2019).

To ensure that the selected targets were amenable to asteroseismic detection from one sector of 30 minutes cadence data, we required that they would have an expected $\nu_{\rm max}$ in the range 30–220 μHz and $T_{\rm eff}$ in the typical range of red giants of 4500–5200 K. In addition, we applied a narrower $T_{\rm eff}$ range of 4500–4700 K for the stars with $\nu_{\rm max}$ between 30 and 70 μHz, to avoid having red clump stars dominating our sample. The resulting sample of stars span evolutionary phases from the base of the red giant branch to the red giant branch bump, as well as some clump stars.

From this sample, we selected the 25 brightest targets for light curve extraction and asteroseismic analysis. The faintest stars in our sample turned out to be ∼6–7th magnitude in the V-band (see Table 1). Under the assumption that the photometric performance of *TESS* is similar to *Kepler*'*s*, apart from its smaller aperture, this magnitude limit is equivalent to 11–12th magnitude for *Kepler*. Because single-quarter observations from *Kepler*'*s* second life, K2, showed no oscillation detection bias for red giants brighter than around twelfth magnitude (Stello et al. 2017), we would expect to detect oscillations in all 25 giants with *TESS*.

Figure 1 illustrates the location of the selected stars in the Hertzsprung–Russell (HR) diagram and the applied selection criteria. We confirmed that the stars were in sectors 1–2 using the Web *TESS* Viewing Tool (WTV).[65]

3. Data Processing and Asteroseismic Analysis

The stars selected were included in an early release of processed data from the TASOC pipeline.[66] The calibrated full-frame images were produced by the *TESS* Science Processing Operations Center (SPOC) at NASA Ames Research Center (Jenkins et al. 2016), and processed by combining the methodology from the K2P2 pipeline (Lund et al. 2015) for extracting the flux from target pixel data with the KASOC filter for systematics correction (Handberg & Lund 2014). The resulting TASOC light curves were high-pass filtered using a filter width of 4 days, corresponding to a cut-off frequency of approximately 3 μHz, and 4σ outliers were removed. Finally, we used linear interpolation to fill gaps that lasted up to three consecutive cadences and derived the Fourier transforms (power frequency spectra) of each light curve.

The light curves for the seven stars observed in both sectors were merged. To follow the approach anticipated for the millions of light curves from the *TESS* full-frame images in the future, we first applied the neural-network-based detection algorithm by Hon et al. (2018) resulting in detection of oscillations in the power spectra of all stars except one. The non-detection (TIC 204314449) is listed as an A2 dwarf and a "Visual Double" in the University of Michigan Catalog of two-dimensional spectral types for the HD stars (Houk 1994), and hence possibly too hot to show solar-like oscillations, or potentially contaminated. For the current test case, the number of stars was small enough that we visually checked the results, which confirmed all detections and the non-detection. The power spectra of a representative sample of the stars are shown in Figure 2, showing clear oscillation excess power and the frequency pattern required to measure both $\nu_{\rm max}$ and $\Delta\nu$.

The neural network also supplies a rough estimate for $\nu_{\rm max}$, which we provided as a prior to 13 independent groups analyzing the power spectra to extract high-precision values of both $\nu_{\rm max}$, $\Delta\nu$, and their respective uncertainties using their preferred method. These methods have been thoroughly tested and described in the literature (see, e.g., Gaulme et al. 2009; Huber et al. 2009; Hekker et al. 2010; Mathur et al. 2010; Mosser et al. 2011; Kallinger et al. 2012; Corsaro & De Ridder 2014; Davies et al. 2016; Campante et al. 2017; Zinn et al. 2019).

From the 13 independent determinations of the global asteroseismic parameters we adopted as central reference value for $\Delta\nu$ and $\nu_{\rm max}$ the results from the pipeline by Gaulme et al. (2009), as this method was on average closest to the ensemble mean after applying a 2σ outlier rejection. Uncertainties in the global asteroseismic parameters obtained by the selected pipeline are at the 1.9% and 2.4% level for $\Delta\nu$ and $\nu_{\rm max}$, respectively. These uncertainties are of comparable magnitude to those obtained from a single campaign with the K2 mission (see the Appendix in Stello et al. 2017) and about twice as large as those extracted from 50 days of *Kepler* observations (see Figures 3 and 4 in Hekker et al. 2012). We report the central values and statistical uncertainties in $\Delta\nu$ and $\nu_{\rm max}$ from the selected pipeline for all targets in Table 1.

For each star, we take into account the scatter across the different methods by adding in quadrature the standard deviation among the central values retained after the 2σ outlier rejection procedure to the formal uncertainty reported by the selected reference method. This consolidation process yields median uncertainties of 3.9% in $\Delta\nu$ and 2.6% in $\nu_{\rm max}$, where the individual contribution arising from this systematic component to the total uncertainty is listed in Table 1. We note that we could decrease the level of uncertainties resulting from our "blind" statistical consolidation approach by for example checking the $\Delta\nu$ and $\nu_{\rm max}$ results against the power spectra and/or échelle diagrams (see Figure 5 in Stello et al. 2011). However, we want to draw a realistic picture of the uncertainties one can expect when dealing with large ensembles of stars (as expected from *TESS*) where detailed "boutique" analysis/checking on a star-by-star basis is not practically feasible. Hence, our quoted uncertainties are conservative, but representative for analysis of *TESS* red giants where several pipelines are involved.

4. Derived Stellar Properties

We have determined stellar properties for a subsample of 17 stars that had spectroscopic measurements of effective temperature and chemical composition available in the literature. As

[65] https://heasarc.gsfc.nasa.gov/cgi-bin/tess/webtess/wtv.py

[66] T'DA Data Release Notes—Data Release 3 for *TESS* Sectors 1+2 (https://doi.org/10.5281/zenodo.2510028).

Table 1
Measured and Derived Stellar Properties of Our Targets

TIC	HIP	$\nu_{\rm max}$ (μHz)	$\Delta\nu$ (μHz)	V (mag)	$T_{\rm eff}$ (K)	[Fe/H] (dex)	R ($R_\odot$)	M ($M_\odot$)	Age (Gyr)	Atmospheric Properties
13097379	114842	59.10 ± 1.50 ± 1.01	6.02 ± 0.03 ± 0.24	6.646 ± 0.010	4634 ± 80	0.04 ± 0.08	8.49 ± 0.28 ± 0.17	1.22 ± 0.08 ± 0.06	6.10 ± 1.06 ± 0.97	Luck (2015)
38574220	19805	29.40 ± 0.90 ± 0.72	4.06 ± 0.20 ± 0.26	5.577 ± 0.009	…	…	…	…	…	…
38828538	21253	189.90 ± 1.60 ± 0.42	14.90 ± 0.10 ± 0.13	5.896 ± 0.009	4828 ± 80	0.11 ± 0.08	4.66 ± 0.10 ± 0.06	1.21 ± 0.05 ± 0.03	6.20 ± 0.50 ± 1.02	Alves et al. (2015)
39082723	4293	49.30 ± 2.10 ± 1.99	5.20 ± 0.10 ± 0.06	5.574 ± 0.009	4706 ± 80	−0.05 ± 0.08	9.30 ± 0.27 ± 0.17	1.19 ± 0.09 ± 0.07	5.90 ± 1.20 ± 1.37	Alves et al. (2015)
47424090	112612	28.30 ± 1.80 ± 1.90	3.40 ± 0.10 ± 0.29	6.930 ± 0.010	…	…	…	…	…	…
70797228	655	31.80 ± 1.50 ± 0.75	4.37 ± 0.20 ± 0.37	5.787 ± 0.009	4750 ± 80	0.12 ± 0.08	11.27 ± 0.61 ± 0.47	1.19 ± 0.13 ± 0.11	6.80 ± 2.20 ± 2.20	Jones et al. (2011)
77116701	103071	48.30 ± 7.60 ± 29.85	5.64 ± 0.20 ± 3.37	8.568 ± 0.018	…	…	…	…	…	…
111750740	113148	142.60 ± 2.70 ± 1.11	11.80 ± 0.10 ± 0.23	5.658 ± 0.009	4688 ± 80	0.16 ± 0.08	5.11 ± 0.16 ± 0.09	1.06 ± 0.07 ± 0.05	10.80 ± 1.78 ± 1.71	Wittenmyer et al. (2016)
115011683	103836	58.80 ± 1.20 ± 0.97	6.10 ± 0.10 ± 0.01	6.057 ± 0.010	4590 ± 80	−0.13 ± 0.08	7.92 ± 0.21 ± 0.22	1.04 ± 0.07 ± 0.07	9.90 ± 1.63 ± 2.01	Wittenmyer et al. (2016)
129649472	105854	31.80 ± 1.20 ± 1.39	4.20 ± 0.20 ± 0.11	5.755 ± 0.009	4748 ± 80	0.28 ± 0.08	10.85 ± 0.60 ± 0.24	1.13 ± 0.12 ± 0.06	8.50 ± 2.76 ± 1.87	Jofré et al. (2015)
139756492	106566	27.60 ± 0.90 ± 0.35	4.16 ± 0.20 ± 0.65	6.819 ± 0.010	…	…	…	…	…	…
141280255	25918	150.40 ± 1.00 ± 0.57	12.52 ± 0.02 ± 0.10	5.307 ± 0.009	4630 ± 80	0.33 ± 0.08	4.98 ± 0.12 ± 0.05	1.07 ± 0.06 ± 0.03	11.70 ± 2.62 ± 2.39	Meléndez et al. (2008)
144335025	117075	68.50 ± 1.60 ± 0.64	7.35 ± 0.20 ± 0.39	6.194 ± 0.010	…	…	…	…	…	…
149347992	26190	165.80 ± 4.10 ± 16.12	11.10 ± 0.40 ± 0.60	6.405 ± 0.010	5132 ± 80	−0.17 ± 0.08	7.20 ± 0.38 ± 0.20	2.17 ± 0.22 ± 0.06	0.80 ± 0.30 ± 0.10	Randich et al. (1999)
155940286	1766	73.20 ± 1.30 ± 0.32	7.40 ± 0.02 ± 0.11	6.810 ± 0.010	4630 ± 80	0.03 ± 0.08	6.95 ± 0.18 ± 0.14	1.01 ± 0.06 ± 0.04	12.00 ± 1.78 ± 36.07	Wittenmyer et al. (2016)
175375523	114775	60.00 ± 1.10 ± 0.30	5.80 ± 0.10 ± 0.14	5.899 ± 0.009	4660 ± 80	0.26 ± 0.08	9.00 ± 0.30 ± 0.58	1.38 ± 0.09 ± 0.21	4.50 ± 0.76 ± 1.35	Jones et al. (2011)
183537408	117659	57.90 ± 1.10 ± 0.80	6.20 ± 0.20 ± 0.42	6.781 ± 0.010	…	…	…	…	…	…
204313960	113801	106.00 ± 3.30 ± 1.47	9.40 ± 0.50 ± 0.43	6.083 ± 0.010	4897 ± 80	−0.20 ± 0.08	6.50 ± 0.18 ± 0.13	1.32 ± 0.07 ± 0.05	3.80 ± 0.57 ± 0.57	Randich et al. (1999)
220517490	12871	117.30 ± 1.20 ± 0.60	10.87 ± 0.02 ± 0.15	5.846 ± 0.009	4961 ± 80	−0.26 ± 0.08	5.61 ± 0.11 ± 0.10	1.10 ± 0.04 ± 0.04	6.10 ± 0.50 ± 1.18	Alves et al. (2015)
237914586	17440	47.00 ± 1.40 ± 1.33	5.74 ± 0.20 ± 0.08	3.959 ± 0.009	…	…	…	…	…	…
270245797	109584	72.20 ± 1.70 ± 0.64	6.60 ± 0.10 ± 0.27	6.239 ± 0.009	4824 ± 80	−0.10 ± 0.08	8.73 ± 0.23 ± 0.39	1.60 ± 0.09 ± 0.13	2.10 ± 0.22 ± 0.64	Alves et al. (2015)
281597433	2789	73.30 ± 1.00 ± 1.37	7.20 ± 0.03 ± 0.19	6.163 ± 0.010	4700 ± 80	−0.41 ± 0.08	6.77 ± 0.15 ± 0.24	0.95 ± 0.05 ± 0.08	11.00 ± 1.35 ± 2.73	Randich et al. (1999)
439399563	343	44.30 ± 1.40 ± 0.66	4.54 ± 0.06 ± 0.11	5.892 ± 0.009	4778 ± 80	0.11 ± 0.08	10.69 ± 0.34 ± 0.40	1.44 ± 0.11 ± 0.14	3.50 ± 0.71 ± 0.78	da Silva et al. (2015)
441387330	102014	46.60 ± 0.80 ± 0.86	5.25 ± 0.10 ± 0.25	5.592 ± 0.009	4710 ± 80	−0.02 ± 0.08	10.18 ± 0.34 ± 0.68	1.40 ± 0.09 ± 0.20	3.40 ± 0.57 ± 1.19	Jones et al. (2011)

Note. Observed V-magnitudes are extracted from the Tycho-2 catalog. The global asteroseismic quantities and stellar properties include a statistical and systematic component derived as described in Sections 3 and 4, respectively. We report them here as $value \pm \sigma_{\rm sta} \pm \sigma_{\rm sys}$. The last column gives the reference from which we retrieved the central values of $T_{\rm eff}$ and [Fe/H] used for the grid-based modeling. Their uncertainties have been homogenized to 80 K and 0.08 dex, respectively (see Section 4).

(This table is available in its entirety in machine-readable form.)

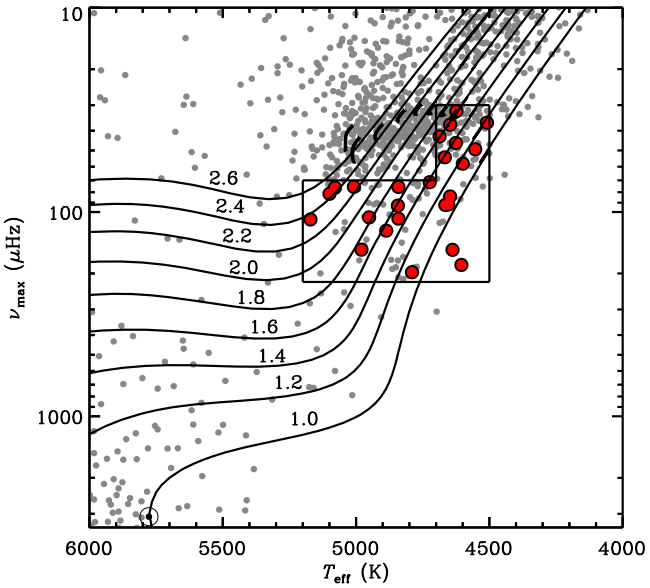

Figure 1. Asteroseismic HR diagram showing (predicted) ν_{max} instead of luminosity. Red dots show the selected targets inside the black selection box. For reference, the Sun is shown as well as all *Hipparcos* stars brighter than sixth magnitude (gray dots). Solar metallicity MESA tracks from Stello et al. (2013) are shown to guide the eye with masses in solar units indicated (pre- and post- helium core-ignition phases are shown separately).

one of our goals is to follow the same analysis procedure expected for large ensembles of stars, we assumed fixed uncertainties in $T_{\rm eff}$ and [Fe/H] of 80 K and 0.08 dex, which are at the level of those provided by current large-scale spectroscopic surveys. To extract the physical properties of our sample, the atmospheric information was complemented with the asteroseismic scaling relations:

$$\left(\frac{\Delta\nu}{\Delta\nu_{\odot}}\right)^2 \simeq \frac{\overline{\rho}}{\overline{\rho}_{\odot}} \quad (1)$$

$$\left(\frac{\nu_{\rm max}}{\nu_{\rm max,\odot}}\right) \simeq \frac{M}{M_{\odot}}\left(\frac{R}{R_{\odot}}\right)^{-2}\left(\frac{T_{\rm eff}}{T_{\rm eff,\odot}}\right)^{1/2}, \quad (2)$$

where we adopted $\Delta\nu_{\odot} = 135.5$ (μHz) and $\nu_{\rm max,\odot} = 3140$ (μHz) as obtained by our reference pipeline from the analysis of solar data.

Seven teams independently applied grid-based modeling pipelines based on stellar evolution models or isochrones to determine the main physical properties of the targets (see Basu et al. 2012; Silva Aguirre et al. 2015; Rodrigues et al. 2017; Mints & Hekker 2018; Yıldız et al. 2019, and references therein). When matching the models to the atmospheric properties and the global asteroseismic parameters $\Delta\nu$ and $\nu_{\rm max}$ the pipelines yielded median uncertainties of ∼6% in radius, ∼14% in mass, and ∼50% in age. These statistical uncertainties are of the same magnitude to those obtained with the K2 mission (Sharma et al. 2019), as expected from the similar resulting errors in the global seismic parameters described in Section 3, and about a factor of two larger than what can be achieved with the full duration of the *Kepler* observations (Pinsonneault et al. 2018).

In addition to the asteroseismic information, five of the pipelines can include parallaxes from *Gaia* DR2 (Gaia Collaboration et al. 2018) coupled with Tycho-2 (Høg et al. 2000) observed *V*-magnitudes in their fitting algorithm to further constrain the stellar properties. As a consequence of having the additional constraint on stellar radius from the astrometry, the resulting uncertainties decrease to a level of ∼3% in radius, ∼6% in mass, and ∼20% in age. This level of precision resembles that obtained with the use of the full length of asteroseismic observations from the nominal *Kepler* mission, and emphasizes the potential of *TESS* for Galactic studies using

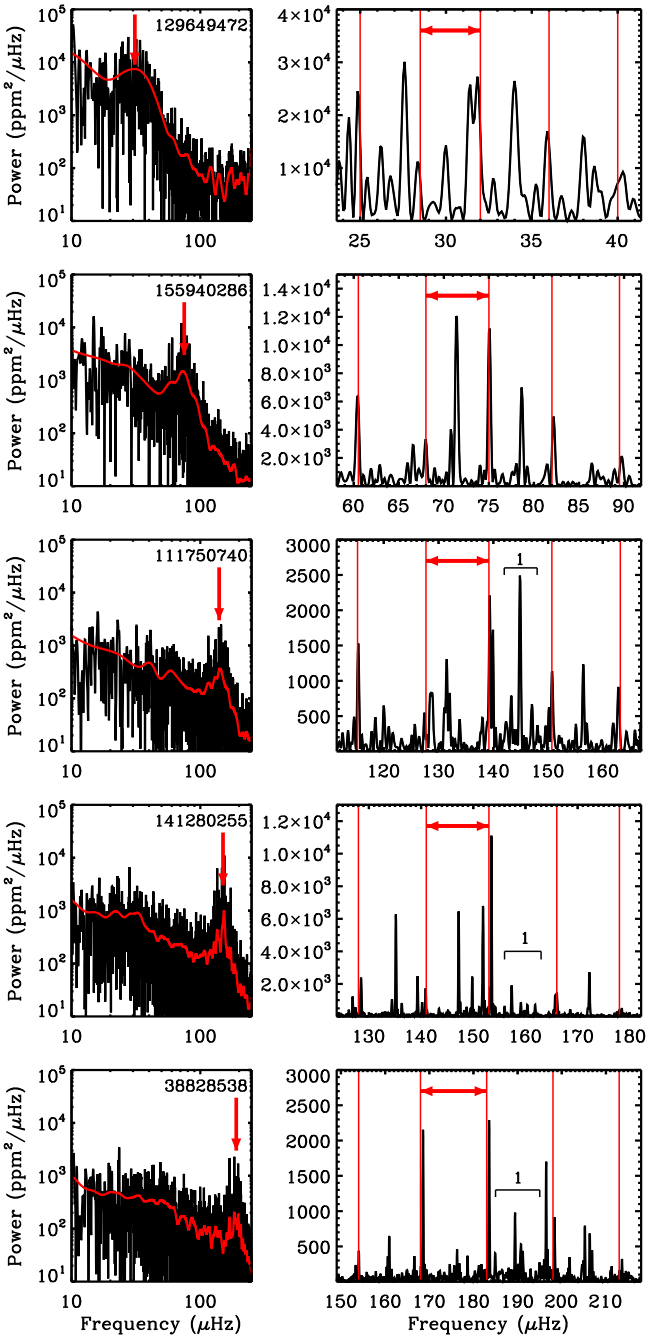

Figure 2. Power spectra sample of our targets representative of the $\nu_{\rm max}$ range that they cover from around the red clump (top) to the low luminosity red giant branch (bottom). Left panels: spectra shown in log–log space (smoothed in red) showing the location of the oscillation power excess, $\nu_{\rm max}$, indicated by red arrows on top of a frequency-dependent granulation background and flat white noise component. Right panels: close-up of spectra showing locations of the roughly equally spaced radial modes (using red equally spaced vertical lines to guide the eye) and their average separation, $\Delta\nu$ (red horizontal arrows). In the three bottom rows multiple dipole ($l = 1$) mixed modes are resolved in between consecutive radial modes as indicated by the black brackets.

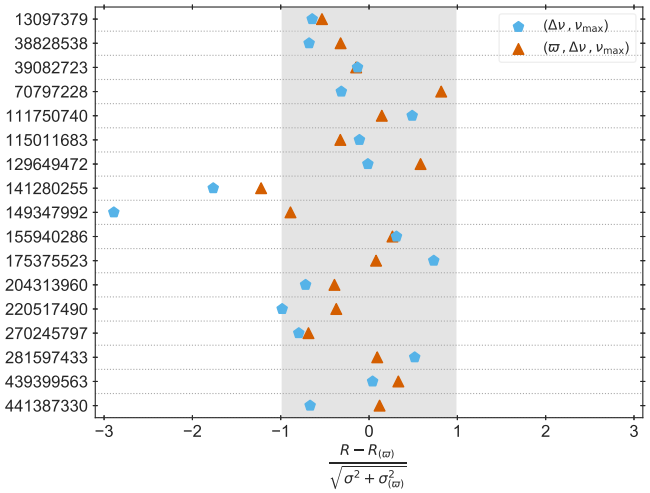

Figure 3. Comparison of stellar radii obtained with BASTA when fitting different combinations of input parameters: *Gaia* DR2 parallax and *V*-band magnitude (ϖ), global asteroseismic parameters ($\Delta\nu$,$\nu_{\rm max}$), and all combined (ϖ,$\Delta\nu$,$\nu_{\rm max}$). Effective temperature and composition are also fitted in all cases. See the text for details.

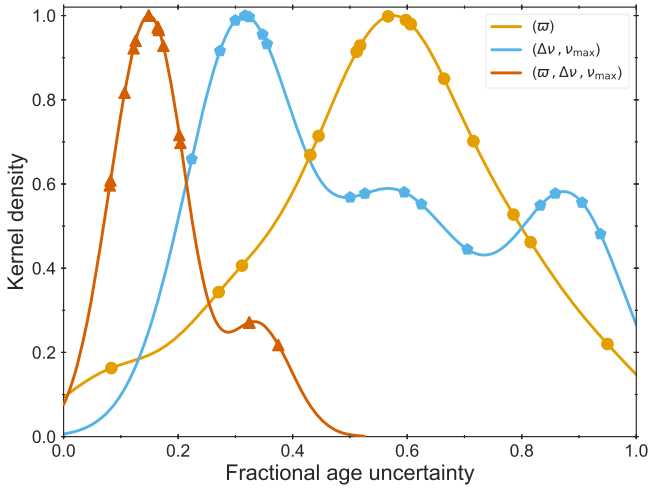

Figure 4. Distribution of fractional age uncertainties for our sample of stars determined by the BASTA pipeline fitting different combinations of available observables. The points indicate the individual values used to construct the Gaussian kernel density estimation. For better visualization we have excluded TIC 175375523 from the figure. See the text for details.

red giants given its larger sky coverage, simple and reproducible selection function, and one order of magnitude higher expected yield of asteroseismic detections than any other previous mission.

To illustrate the differences in the obtained stellar properties arising from the selection of fitted observables, Figure 3 shows the stellar radius obtained with one of the pipelines (BASTA; Silva Aguirre et al. 2015) when fitting different combinations of input parameters. The figure uses as the reference value the case when, in addition to the atmospheric properties, only the *Gaia* DR2 parallax and observed *V*-band magnitude are included in the fit. For the majority of the targets the results are consistent across the three sets within their formal statistical uncertainties. A summary of the measured and derived stellar properties for our targets can be found in Table 1, where we have listed the central values and statistical uncertainties obtained with the BASTA pipeline, and determined the systematic contribution as the standard deviation across the results reported by all pipelines.

Two targets (TIC 141280255 and TIC 149347992) present a larger disagreement between the radii obtained with parallax and the seismic set ($\Delta\nu$, $\nu_{\rm max}$). We investigated whether these discrepancies were due to the quality of the astrometric data by computing the re-normalized unit weight error (RUWE)[67] for our sample of stars. In the case of TIC 141280255 we obtained a RUWE = 1.98, which is above the value recommended by the *Gaia* team as a criterion for a good astrometric solution (RUWE $\leqslant$ 1.4). Therefore, we adopt for this star the stellar properties obtained from fitting the asteroseismic input only ($\Delta\nu$, $\nu_{\rm max}$).

In the case of TIC 149347992 the discrepancy is the result of predicted evolutionary phases: while the parallax-only solution suggests that the star in the clump phase, the asteroseismic fit favors a star in the red giant branch. The combined fit therefore presents a bimodal distribution that encompasses these two families of solutions. A similar situation occurs in the fit of TIC 175375523, which shows agreement in the radius determined from different sets of input but has a fractional age uncertainty above unity when only ($\Delta\nu$, $\nu_{\rm max}$) are included in the fit. Its resulting age distribution is bimodal in this set as both red giant branch and clump models can reproduce the observations, but the inclusion of parallax information favors the red giant branch solution and accounts for the $\sim$17% statistical uncertainty reported in Table 1. The availability of evolutionary classifications from deep neural networks trained on short *Kepler* data (Hon et al. 2018) would further decrease the obtained uncertainties by clearly disentangling these two scenarios.

In Figure 4 we plot the distribution of fractional age uncertainties obtained with BASTA for the three considered cases of input, showing the clear improvement in precision when asteroseismic information and parallax are simultaneously included in the fit. For visualization purposes we have excluded the target TIC 175375523 from the figure. Our stellar ages at the 20% level are significantly more precise than what is obtained by data-driven and neural-network methods trained using asteroseismic ages from *Kepler* (above the 30% level, see e.g., Mackereth et al. 2019). As a final remark, we note that asteroseismically derived properties of red giants are accurate to at least a similar level than our statistical uncertainties (below $\sim$5% and $\sim$10% for radii and masses, respectively; see the discussion in e.g., Pinsonneault et al. 2018, and references therein). We have made emphasis on our achieved precision instead of accuracy as our results could still be affected by a systematic component arising from uncertainties in evolutionary calculations, although recent investigations quantifying these effects at solar metallicity suggest that they are smaller than our statistical uncertainties (Silva Aguirre et al. 2019).

5. Conclusions

We presented the first ensemble analysis of red giant stars observed with the *TESS* mission. We selected a sample of 25 stars where we expected to detect oscillations based on their magnitude and parallax value, and analyzed the extracted light curves in search for asteroseismic signatures in the power spectra. Our main findings can be summarized as follows.

[67] See *Gaia* technical note GAIA-C3-TN-LU-LL-124-01 (https://www.cosmos.esa.int/web/gaia/dr2-known-issues).

1. We detected oscillations in all the stars (except one that was likely incorrectly listed as a red giant). Despite the modest number of stars in our sample, our detection yield supports that the *TESS* photometric performance is similar to that of *Kepler* and K2 except shifted by about 5 magnitudes toward brighter stars due to its smaller aperture.
2. Individual pipelines retrieve the global asteroseismic parameters with uncertainties at the ∼2% level in $\Delta\nu$ and ∼2.5% in $\nu_{\rm max}$, which, respectively, increase to ∼4% and ∼3.5% when we take into account the scatter across results. We consider these uncertainties to be representative for the forthcoming ensemble analysis of *TESS* targets observed in 1–2 sectors, as individual validation of the results will not be feasible due to the large number of targets observed.
3. Grid-based modeling techniques applying asteroseismic scaling relations were used to retrieve stellar properties for the 17 targets with spectroscopic information. Radii, masses, and ages were obtained with uncertainties at the 6%, 14%, and 50% level, and decrease to 3%, 6%, and 20% when parallax information from *Gaia* DR2 is included.

The expected number of red giants with detected oscillations by *TESS* (∼500,000[68]) greatly surpasses the final yield of *Kepler* (∼20,000). In this respect, the combination of *TESS* observations, *Gaia* astrometry, and large-scale spectroscopic surveys holds a great potential for studies of Galactic structure where precise stellar properties (particularly ages) are of key importance. We note that the recently approved extended *TESS* mission will change the 30 minutes cadence to 10 minutes, making it possible to detect oscillations of stars of smaller radii using the full-frame images. This will enable more rigorous investigations of the asteroseismic mass scale for giants when anchored to empirical mass determinations (e.g., from eclipsing binaries) of turn-off and subgiant stars.

This Letter includes data collected by the *TESS* mission, which are publicly available from the Mikulski Archive for Space Telescopes (MAST). Funding for the *TESS* mission is provided by NASA's Science Mission directorate. Funding for the *TESS* Asteroseismic Science Operations Centre is provided by the Danish National Research Foundation (grant agreement No. DNRF106), ESA PRODEX (PEA 4000119301), and Stellar Astrophysics Centre (SAC) at Aarhus University. V.S.A. acknowledges support from the Independent Research Fund Denmark (Research grant 7027-00096B). D.B. is supported in the form of work contract FCT/MCTES through national funds and by FEDER through COMPETE2020 in connection to these grants: UID/FIS/04434/2019; PTDC/FIS-AST/30389/2017 & POCI-01-0145-FEDER-030389. L.B., R.A.G., and B.M. acknowledge the support from the CNES/PLATO grant. D.B. acknowledges NASA grant NNX16AB76G. T.L.C. acknowledges support from the European Union's Horizon 2020 research and innovation programme under the Marie Skłodowska-Curie grant agreement No. 792848 (PULSATION). This work was supported by FCT/MCTES through national funds (UID/FIS/04434/2019). E.C. is funded by the European Union's Horizon 2020 research and innovation program under the Marie Skłodowska-Curie grant agreement No. 664931. R.H. and M.N.L. acknowledge the support of the ESA PRODEX programme. T.S.R. acknowledges financial support from Premiale 2015 MITiC (PI B. Garilli). K.J.B. is supported by the National Science Foundation under Award AST-1903828. M.S.L. is supported by the Carlsberg Foundation (grant agreement No. CF17-0760). M.C. is funded by FCT//MCTES through national funds and by FEDER through COMPETE2020 through these grants: UID/FIS/04434/2019, PTDC/FIS-AST/30389/2017 & POCI-01-0145-FEDER-030389, CEECIND/02619/2017. The research leading to the presented results has received funding from the European Research Council under the European Community's Seventh Framework Programme (FP7/2007-2013)/ERC grant agreement no 338251 (StellarAges). A.M. acknowledges support from the European Research Council Consolidator Grant funding scheme (project ASTEROCHRONOMETRY, grant agreement No. 772293, http://www.asterochronometry.eu). A.M.S. is partially supported by MINECO grant ESP2017-82674-R. J.C.S. acknowledges funding support from Spanish public funds for research under projects ESP2017-87676-2-2, and from project RYC-2012-09913 under the 'Ramón y Cajal' program of the Spanish Ministry of Science and Education. Resources supporting this work were provided by the NASA High-End Computing (HEC) Program through the NASA Advanced Supercomputing (NAS) Division at Ames Research Center for the production of the SPOC data products.

[68] Based on a preliminary simulation of the full TESS sky (*TESS* GI Proposal No. G011188).

ORCID iDs

Víctor Silva Aguirre https://orcid.org/0000-0002-6137-903X
Dennis Stello https://orcid.org/0000-0002-4879-3519
Amalie Stokholm https://orcid.org/0000-0002-5496-365X
Jakob R. Mosumgaard https://orcid.org/0000-0001-9234-430X
Warrick H. Ball https://orcid.org/0000-0002-4773-1017
Sarbani Basu https://orcid.org/0000-0002-6163-3472
Diego Bossini https://orcid.org/0000-0002-9480-8400
Lisa Bugnet https://orcid.org/0000-0003-0142-4000
Derek Buzasi https://orcid.org/0000-0002-1988-143X
Tiago L. Campante https://orcid.org/0000-0002-4588-5389
Lindsey Carboneau https://orcid.org/0000-0003-1001-5137
William J. Chaplin https://orcid.org/0000-0002-5714-8618
Enrico Corsaro https://orcid.org/0000-0001-8835-2075
Guy R. Davies https://orcid.org/0000-0002-4290-7351
Rafael A. García https://orcid.org/0000-0002-8854-3776
Patrick Gaulme https://orcid.org/0000-0001-8330-5464
Oliver J. Hall https://orcid.org/0000-0002-0468-4775
Rasmus Handberg https://orcid.org/0000-0001-8725-4502
Marc Hon https://orcid.org/0000-0003-2400-6960
Thomas Kallinger https://orcid.org/0000-0003-3627-2561
Liu Kang https://orcid.org/0000-0001-5219-7894
Mikkel N. Lund https://orcid.org/0000-0001-9214-5642
Savita Mathur https://orcid.org/0000-0002-0129-0316
Alexey Mints https://orcid.org/0000-0002-8440-1455
Benoit Mosser https://orcid.org/0000-0002-7547-1208
Zeynep Çelik Orhan https://orcid.org/0000-0002-9424-2339
Thaíse S. Rodrigues https://orcid.org/0000-0002-9414-339X
Mutlu Yıldız https://orcid.org/0000-0002-7772-7641
Joel C. Zinn https://orcid.org/0000-0002-7550-7151
Sibel Örtel https://orcid.org/0000-0001-5759-7790

Paul G. Beck https://orcid.org/0000-0003-4745-2242
Keaton J. Bell https://orcid.org/0000-0002-0656-032X
Zhao Guo https://orcid.org/0000-0002-0951-2171
Chen Jiang https://orcid.org/0000-0002-7614-1665
James S. Kuszlewicz https://orcid.org/0000-0002-3322-5279
Marc Pinsonneault https://orcid.org/0000-0002-7549-7766
Jamie Tayar https://orcid.org/0000-0002-4818-7885
Margarida S. Cunha https://orcid.org/0000-0001-8237-7343
Saskia Hekker https://orcid.org/0000-0002-1463-726X
Andrea Miglio https://orcid.org/0000-0001-5998-8533
Mario J. P. F. G. Monteiro https://orcid.org/0000-0003-0513-8116
Ditte Slumstrup https://orcid.org/0000-0003-4538-9518
George Angelou https://orcid.org/0000-0003-4463-1907
Othman Benomar https://orcid.org/0000-0001-9405-5552
Aliz Derekas https://orcid.org/0000-0002-6526-9444
Maria Pia Di Mauro https://orcid.org/0000-0001-7801-7484
Yveline Lebreton https://orcid.org/0000-0002-4834-2144
Jaymie Matthews https://orcid.org/0000-0002-4461-080X
Nicolas Nardetto https://orcid.org/0000-0002-7399-0231
Jose D. do Nascimento, Jr. https://orcid.org/0000-0001-7804-2145
Filipe Pereira https://orcid.org/0000-0002-2157-7146
Luisa F. Rodríguez Díaz https://orcid.org/0000-0002-0588-1375
Emanuele Spitoni https://orcid.org/0000-0001-9715-5727
Vincent Van Eylen https://orcid.org/0000-0001-5542-8870
Rita Ventura https://orcid.org/0000-0002-5152-0482
Kuldeep Verma https://orcid.org/0000-0003-0970-6440
Achim Weiss https://orcid.org/0000-0002-3843-1653
Tao Wu https://orcid.org/0000-0001-6832-4325
Thomas Barclay https://orcid.org/0000-0001-7139-2724
Jørgen Christensen-Dalsgaard https://orcid.org/0000-0001-5137-0966
Jon M. Jenkins https://orcid.org/0000-0002-4715-9460
Sara Seager https://orcid.org/0000-0002-6892-6948
Roland Vanderspek https://orcid.org/0000-0001-6763-6562

References

Alves, S., Benamati, L., Santos, N. C., et al. 2015, MNRAS, 448, 2749
Anders, F., Chiappini, C., Rodrigues, T. S., et al. 2017, A&A, 597, A30
Basu, S., Verner, G. A., Chaplin, W. J., & Elsworth, Y. 2012, ApJ, 746, 76
Bedding, T. R., Huber, D., Stello, D., et al. 2010, ApJL, 713, L176
Bedding, T. R., Mosser, B., Huber, D., et al. 2011, Natur, 471, 608
Campante, T. L., Corsaro, E., Lund, M. N., et al. 2019, ApJ, 885, 31
Campante, T. L., Veras, D., North, T. S. H., et al. 2017, MNRAS, 469, 1360
Casagrande, L., Silva Aguirre, V., Schlesinger, K. J., et al. 2016, MNRAS, 455, 987
Corsaro, E., & De Ridder, J. 2014, A&A, 571, A71
da Silva, R., Milone, A. d. C., & Rocha-Pinto, H. J. 2015, A&A, 580, A24
Davies, G. R., Silva Aguirre, V., Bedding, T. R., et al. 2016, MNRAS, 456, 2183
Flower, P. J. 1996, ApJ, 469, 355
Gaia Collaboration, Katz, D., Antoja, T., et al. 2018, A&A, 616, A11
Gaulme, P., Appourchaux, T., & Boumier, P. 2009, A&A, 506, 7
Handberg, R., & Lund, M. N. 2014, MNRAS, 445, 2698
Hekker, S., Broomhall, A.-M., Chaplin, W. J., et al. 2010, MNRAS, 402, 2049
Hekker, S., Elsworth, Y., Mosser, B., et al. 2012, A&A, 544, A90
Høg, E., Fabricius, C., Makarov, V. V., et al. 2000, A&A, 355, L27
Hon, M., Stello, D., & Yu, J. 2018, MNRAS, 476, 3233
Houk, N. 1994, in ASP Conf. Ser. 60, The MK Process at 50 years: A Powerful Tool for Astrophysical Insight, ed. C. Corbally, R. O. Gray, & R. F. Garrison (San Francisco, CA: ASP), 285
Huber, D., Stello, D., Bedding, T. R., et al. 2009, CoAst, 160, 74
Jenkins, J. M., Twicken, J. D., McCauliff, S., et al. 2016, Proc. SPIE, 9913, 99133E
Jofré, E., Petrucci, R., Saffe, C., et al. 2015, A&A, 574, A50
Jones, M. I., Jenkins, J. S., Rojo, P., & Melo, C. H. F. 2011, A&A, 536, A71
Kallinger, T., Hekker, S., Mosser, B., et al. 2012, A&A, 541, 51
Luck, R. E. 2015, AJ, 150, 88
Lund, M. N., Handberg, R., Davies, G. R., Chaplin, W. J., & Jones, C. D. 2015, ApJ, 806, 30
Mackereth, J. T., Bovy, J., Leung, H. W., et al. 2019, MNRAS, 489, 176
Mathur, S., García, R. A., Régulo, C., et al. 2010, A&A, 511, 46
Meléndez, J., Asplund, M., Alves-Brito, A., et al. 2008, A&A, 484, L21
Miglio, A., Chiappini, C., Morel, T., et al. 2013, MNRAS, 429, 423
Miglio, A., Montalbán, J., Baudin, F., et al. 2009, A&A, 503, L21
Mints, A., & Hekker, S. 2018, A&A, 618, A54
Mosser, B., Elsworth, Y., Hekker, S., et al. 2011, A&A, 537, A30
Pinsonneault, M. H., Elsworth, Y. P., Tayar, J., et al. 2018, ApJS, 239, 32
Randich, S., Gratton, R., Pallavicini, R., Pasquini, L., & Carretta, E. 1999, A&A, 348, 487
Ricker, G. R., Winn, J. N., Vanderspek, R., et al. 2015, JATIS, 1, 014003
Rodrigues, T. S., Bossini, D., Miglio, A., et al. 2017, MNRAS, 467, 1433
Sharma, S., Stello, D., Bland-Hawthorn, J., et al. 2019, MNRAS, 490, 5335
Silva Aguirre, V., Bojsen-Hansen, M., Slumstrup, D., et al. 2018, MNRAS, 475, 5487
Silva Aguirre, V., Christensen-Dalsgaard, J., Cassisi, S., et al. 2019, arXiv:1912.04909
Silva Aguirre, V., Davies, G. R., Basu, S., et al. 2015, MNRAS, 452, 2127
Stello, D., Huber, D., Bedding, T. R., et al. 2013, ApJL, 765, L41
Stello, D., Meibom, S., Gilliland, R. L., et al. 2011, ApJ, 739, 13
Stello, D., Zinn, J., Elsworth, Y., et al. 2017, ApJ, 835, 83
Van Leeuwen, F. 2007, A&A, 474, 653
Wittenmyer, R. A., Liu, F., Wang, L., et al. 2016, AJ, 152, 19
Yıldız, M., Çelik Orhan, Z., & Kayhan, C. 2019, MNRAS, 489, 1753
Yu, J., Huber, D., Bedding, T. R., et al. 2018, ApJS, 236, 42
Zinn, J. C., Stello, D., Huber, D., & Sharma, S. 2019, ApJ, 884, 107